JOURNAL OF MATERIALS SCIENCE 31 (1996) 995–1004

Quantitative phase analysis of metastable structure in a laser melted Fe–C alloy

Part II *Structural analysis of overlapping tracks by X-ray diffraction*

M. ČERŇANSKÝ, J. ČERMÁK, N. ZÁRUBOVÁ, P. WOLF
Institute of Physics, Academy of Sciences of the Czech Republic, Na Slovance 2, CZ-180 40 Praha 8, Czech Republic

---

Quantitative X-ray diffraction phase analysis was utilized to investigate the structure of a Fe–3.5 wt% C alloy after laser melting. The measurements were taken on surfaces modified by a series of equidistant laser tracks with overlappings $k = 0.25, 0.50$ and 0.75, and the results were extrapolated to the non-interfering tracks. On the same samples, the microstructure was observed by scanning electron microscopy. The structure of the rapidly solidified surface layers consists of α-Fe (ferrite and martensite), γ-Fe (retained austenite) and cementite. The results of X-ray diffraction point to a very high amount of carbide indicating a non-stoichiometric composition of cementite. Besides, the volume fraction of α-Fe increases with increasing coefficient of overlapping k. At the same time, the volume fraction of cementite decreases while the content of γ-Fe remains nearly constant. The changes are attributed to decomposition of the metastable carbide due to tempering of the former tracks by the following laser passes. This thermal effect was quantified on the base of the heat-transfer model of moving Gaussian beam.

---

1. Introduction

It is evident that the attractive properties of laser treated materials, e.g. enhanced hardness, improved wear and corrosion resistance, result from specific structures formed in the surface layers during laser irradiation. As a consequence of extreme heating and cooling rates highly refined structures, high solid supersaturations, metastable phases, new microstructures (such as banding phenomena [1]) etc. can occur. In order to understand the non-equilibrium processes which can take place in the laser treated as well as other rapidly quenched materials, it is highly desirable to have a detailed quantitative characterization of the resulting structures.

The aim of this paper is to describe the method and results of a quantitative X-ray diffraction phase analysis applied to a laser melted Fe–3.5 wt% C alloy. X-ray diffraction has been sporadically used to analyse individual as well as superimposed laser tracks. However, the method has been used mostly to measure residual stresses [2–8] or to perform a qualitative identification of the structural components [3, 9–11]. Quantitative X-ray diffraction phase analysis of the laser treated surface layers is a rather complicated task requiring measurements of integral intensities of individual diffraction lines, or more frequently of groups of lines, with a precision as high as possible.

Test diffraction patterns on single laser tracks of the breadth of several tenths of mm produced diffraction lines of some components of a very clear spotty character* so that this procedure could not be used for reliable intensity measurements. Another combination appeared more promising, i.e. to analyse a series of parallel overlapping laser tracks representing an area of practically arbitrary dimensions according to the parameters of the programmed movement of the laser beam across the sample. In this way diffraction lines of good quality for intensity measurements may be obtained. The procedure offers furthermore the opportunity to use a different extent of overlapping between successive laser passes and to estimate the heat effect of adjacent passes on the preceding ones. An extrapolation may lead to a phase composition of non-interfering individual tracks.

The analytical procedure applied in this study presents as the final result the quantitative structural

---

*Smooth, continuous diffraction lines may convert into discrete diffraction spots from individual diffracting particles (crystallites). It is a consequence of having too small a number of diffracting particles in the volume irradiated by X-rays. The phenomenon of spottiness of diffraction lines occurs usually in the case of substances with large particles ($> 10^{-3}$ mm), lower crystalline symmetry, i.e. small multiplicity factor of reflecting planes, high absorption and with immobile samples during the exposure.

composition of an extended laser melted surface which is certainly more representative of treatments in practical applications. Moreover, the extrapolation data allow for correlation of the X-ray diffraction results with the metallurgical investigations of individual tracks as described in Part I of this paper.

2. Experimental techniques

Details concerning the starting material (pure Fe–3.5 wt% C alloy) and the laser irradiation experiments were given in Part I where single melted tracks were treated. In this part we shall concentrate on superimposed tracks. The laser beam moved over the specimen surface at speeds $v = 8.5$ and $17\ \mathrm{cm\,s^{-1}}$ (at higher scanning speeds the original structure was not completely melted; at $v = 4\ \mathrm{cm\,s^{-1}}$ the sample surface was too rough for X-ray measurements) and the tracks overlapped by 0.25, 0.50 and 0.75 of the melt-zone width. A detailed structural investigation was performed by X-ray diffraction measurements and supplemented with observations by scanning electron microscopy (SEM).

The X-ray diffraction patterns were obtained in a semi-focusing Bragg–Brentano camera of diameter 114 mm. Radiation FeK_α was monochromated by a bent quartz crystal with Johannsson geometry. The radius of the focal circle was 250 mm and the reflection 0 1 1 ($0 1 \bar{1} 1$) was utilized with diffraction angle $\vartheta_0 = 16.8°$. The angle of incidence of the primary beam to the specimen surface was $\alpha = 40°$. The diffracting area on the sample surface was approximately $3 \times 1.5\ \mathrm{mm}^2$ and the exposures were 40 to 120 h. Both stationary and rotating samples were exposed. Diffraction patterns of the stationary samples indicated the extent of texture and in some cases also spotty lines. The rotation of samples eliminated the spottiness of the diffraction lines and suppressed the influence of texture.

The SEM observations were made on nital etched cross-sections of the overlapping tracks. In addition, specimen surfaces were observed in detail after slight grinding, polishing and etching.

3. Quantitative X-ray diffraction phase analysis

The recorded diffraction lines could be indexed as ferrite, austenite and cementite. No other phases were identified. In spite of the fact that only three phases were present in the investigated layers, the diffraction patterns contained a great number of diffraction lines, many of them overlapping. Nevertheless, it was possible to select eleven mutually separated groups of overlapping lines in the angle range 20–80°. These eleven compound lines contained all four reflections of ferrite, all five reflections of austenite, and many reflections of cementite. Cementite gives theoretically with the radiation Fe as much as 130 reflections. The first eight of them with the diffraction angle $\vartheta < 20°$ were screened by the specimen. The intensities of many others were very low so that altogether 43 diffraction lines of cementite could be taken into account.

Quantitative X-ray diffraction phase analysis is based on the relation, see e.g. [12–14]:

$$I'_{ij} = L\,\Phi_i B'_{ij} \tag{1}$$

where L is a constant which is the same for all phases in the sample and for all reflections in the diffraction pattern, Φ_i is the volume fraction of the ith phase, I'_{ij} is the integral intensity of the jth reflection of the ith phase and B'_{ij} is the corresponding intensity factor. The relation for B'_{ij} follows from the well known relation for the integral intensity of X-ray diffraction of polycrystalline materials, see e.g. [12, 13].

In Table I calculated diffraction angles ϑ and intensity factors B for selected reflections of the identified phases are summarized. The input data were: the wavelength of the iron radiation $\lambda_{K_{\alpha_1}} = 0.193597$ nm; the lattice parameter of ferrite $a = 0.28663$ nm; the lattice parameter of austenite $a = 0.36467$ nm; the lattice parameters of cementite $a = 0.45230$ nm, $b = 0.50890$ nm and $c = 0.67428$ nm [15]. Using these values, the theoretical densities of ferrite ($7.88\ \mathrm{g\,cm^{-3}}$), austenite ($7.65\ \mathrm{g\,cm^{-3}}$) and cementite ($7.68\ \mathrm{g\,cm^{-3}}$) were estimated. For the average density of the samples a value of $7.79\ \mathrm{g\,cm^{-3}}$ was obtained. The presence of the carbon atoms in ferrite and austenite was neglected in the calculations. Similarly the linear absorption coefficient $\mu = 550.2\ \mathrm{cm^{-1}}$ was calculated under the assumption that only cementite and pure α-Fe were present in the samples. In contrast to the Bragg–Brentano goniometer, the absorption factor A for the Bragg–Brentano semi-focusing camera is angular dependent. This fact was respected also in the calculations of the intensity factors and the following relation [16] was used

$$A = \frac{1}{\mu}\,\frac{\sin(2\vartheta - \alpha)}{\sin(2\vartheta - \alpha) + \sin\alpha} \tag{2}$$

where ϑ is the diffraction angle of the chosen line and α is the angle of incidence of the primary beam on the surface of the sample. It is apparent that the angular dependent part of the absorption factor can be easily separated and included in the intensity factors. The linear absorption coefficient μ of the sample can be included in the common constant L. The intensity factors given in Table I were calculated according to the relation:

$$B'_{ij} = \frac{n|F_{ij}|^2}{(V_i^c)^2}\,\frac{1}{\sin^2\vartheta_{ij}\cos\vartheta_{ij}}\,\frac{1 + \cos^2 2\vartheta_0 \cos^2 2\vartheta_{ij}}{1 + \cos^2 2\vartheta_0} \times \frac{\sin(2\vartheta_{ij} - \alpha)}{\sin(2\vartheta_{ij} - \alpha) + \sin\alpha} \tag{3}$$

where suffixes i, j refer to the phase and to the reflection, respectively, n is the multiplicity factor, F is the structure factor (non-corrected for the temperature factor), V_i^c is the volume of the elementary cell of the ith phase. If several reflections of the same phase contribute to the integral intensity of a compound line, the sum of the intensity factors B'_{ij} is taken as the intensity factor B_{ij}. As seen from Table I, this was the case for the reflections of cementite. This procedure is justified by the direct proportion in the Relation 1. Any additional corrections [17] of B_{ij} were not done.

TABLE I Calculated parameters of selected reflections of the analysed phases

Compound line	Phase	*hkl*	ϑ (°)	B'_{ij} (arb. units)	B_{ij} (arb. units)
1	ferrite	110	28.529	25.8725	25.8725
	austenite	111	27.372	16.6645	16.6645
	cementite	121	27.354	2.2262	13.6632
	”	210	27.930	2.1944	”
	”	022	28.464	2.2173	”
	”	103	28.745	4.6255	”
	”	211	29.334	2.3998	”
2	austenite	200	32.065	10.6576	10.6576
	cementite	202	31.025	0.0652	5.8965
	”	113	31.142	1.6759	”
	”	122	31.497	3.0073	”
	”	212	33.325	1.1481	”
3	cementite	130	37.550	1.1408	1.1805
	”	123	37.821	0.0397	”
4	ferrite	200	42.487	6.9512	6.9512
	cementite	301	41.140	0.0121	0.6051
	”	132	42.353	0.0323	”
	”	311	43.223	0.1986	”
	”	024	43.536	0.3621	”
5	austenite	220	48.658	10.8456	10.8456
	cementite	133	48.268	0.0602	0.2691
	”	320	48.270	0.0101	”
	”	105	48.505	0.1988	”
6	cementite	140	52.220	1.8733	6.0003
	”	313	52.765	2.3764	”
	”	322	53.093	0.0155	”
	”	141	53.447	0.3690	”
	”	224	54.191	0.1542	”
	”	025	54.328	1.0073	”
	”	042	54.411	0.2046	”
7	ferrite	211	55.814	21.2310	21.2310
	cementite	233	56.434	2.9686	5.0172
	”	134	56.862	0.1153	”
	”	125	57.149	1.8257	”
	”	142	57.236	0.1076	”
8	cementite	400	58.877	0.3755	5.6920
	”	215	58.992	1.7433	”
	”	330	59.202	2.3554	”
	”	006	59.468	1.2178	”
9	austenite	311	61.687	20.8734	20.8734
	cementite	331	60.562	0.4086	5.4925
	”	043	60.960	2.3716	”
	”	410	61.275	1.2077	”
	”	314	61.900	0.7587	”
	”	411	62.699	0.7459	”
10	austenite	222	66.855	7.7604	7.7604
	cementite	234	66.311	0.2032	1.7478
	”	225	66.669	0.8810	”
	”	242	66.778	0.2674	”
	”	412	67.330	0.3962	”
11	ferrite	220	72.784	15.2812	15.2812
	cementite	044	72.406	0.0724	0.0724

The measured intensities I_j ($j = 1, 2, \ldots, m$) of the selected compound lines represent the right hand sides in the system of equations, see e.g. [18, 19]

$$B_{1j}L\Phi_1 + B_{2j}L\Phi_2 + B_{3j}L\Phi_3 = I_j \qquad (j = 1, 2, \ldots, m) \qquad (4)$$

quantities j and m respectively, are now index and number of the actual considered compound lines in the calculations.

The volume fraction of the ith phase, Φ_i, can be easily estimated from the relation:

$$\Phi_i = \frac{L\Phi_i}{L\Phi_1 + L\Phi_2 + L\Phi_3} \quad (i = 1, 2, 3) \quad (5)$$

provided that the Equation system 4 for the unknown $L\Phi_i$ has been solved.

If the number m of the compound lines or equations in 4 is higher than the number of phases, the System 4 is overestimated and can be transformed by well known algebraic methods into a system (see e.g. [18]).

$$
\begin{aligned}
&Lw_1 \sum_{j=1}^{m} B_{1j}^2 + Lw_2 \sum_{j=1}^{m} B_{1j}B_{2j} \\
&\quad + Lw_3 \sum_{j=1}^{m} B_{1j}B_{3j} = \sum_{j=1}^{m} I_j B_{1j}, \\
&Lw_1 \sum_{j=1}^{m} B_{1j}B_{2j} + Lw_2 \sum_{j=1}^{m} B_{2j}^2 \\
&\quad + Lw_3 \sum_{j=1}^{m} B_{2j}B_{3j} = \sum_{j=1}^{m} I_j B_{2j}, \qquad (6) \\
&Lw_1 \sum_{j=1}^{m} B_{1j}B_{3j} + Lw_2 \sum_{j=1}^{m} B_{2j}B_{3j} \\
&\quad + Lw_3 \sum_{j=1}^{m} B_{3j}^2 = \sum_{j=1}^{m} I_j B_{3j}
\end{aligned}
$$

for the unknown $L\Phi_i$.

4. Experimental results

4.1. X-ray diffraction

Distinct diffraction lines of ferrite were well visible on the diffraction patterns and corresponding photometer records. The lines of austenite were weaker. The ferrite and austenite lines were surrounded by numerous diffraction lines of cementite. On the other hand, diffraction lines of martensite were not found though martensite needles are clearly discernible in the SEM and TEM micrographs (see Figs 3c and 4a in Part I). A similar case was described in [20]. The search for ε-carbide [21] and hexagonal ε-phase [22–25] also failed even though at least four diffraction patterns were analysed for each scanning speed and coefficient of overlapping.

Table II summarizes measured integral intensities I of the eleven selected compound lines from the best series of the diffraction patterns. The input data for the values given in Table II were tested by preliminary computations taking various combinations of the diffraction lines. First of all it was found that the intensity of the diffraction lines with small diffraction angles (the first, second and third lines) was evidently influenced by the surface roughness. For this reason we tried to take diffraction patterns also from samples with slightly ground and polished surfaces. However, the quality of the lines with low ϑ did not improve so that these lines were excluded from further processing. Moreover, the 3rd line (reflections 130 and 123 of cementite) was more appreciably influenced by texture. The 6th and 7th lines had to be omitted as well because their separation and consequently the estimation of the background was rather questionable. Similarly the 11th line was not taken into account because it was very broad and weak. When using the described method of phase analysis working with compound diffraction lines, it is further to be recommended not to choose compound lines with very different diffraction angles and not to make use of too many compound lines. Finally, it is not convenient when the individual compound lines cover intervals of diffraction angles that are too broad.

On the basis of this experience a combination of the compound lines 4, 5, 8, 9, 10 was chosen, i.e. only five from all eleven compound lines. Here the fourth line contains reflection 200 of ferrite, the fifth, ninth and tenth lines contain reflections 220, 311 and 222 of austenite and each of the selected compound lines includes several reflections of cementite. Results of the quantitative diffraction phase analysis are given in Table III.

4.2. Microscopic observations

A typical cross-sectional view of the overlapping tracks is shown in Fig. 1. The structure is nearly identical with that observed on single tracks (see Figs 3 and 4 in Part I). The only pronounced difference in the microstructure morphology was observed in the narrow (~ 10–12 μm) "mushy zone" where the temperature during the subsequent pass was between the solidus and liquidus temperatures. The situation is shown in detail in Fig. 2. In this zone the secondary dendrite arms have nearly disappeared and the dendrites are often equiaxed and relatively coarse. The reason is as follows: between liquidus and solidus

TABLE II Measured integral intensities for the selected 11 compound lines

Group of lines	$v = 8.5$ cm s^{-1}			$v = 17.0$ cm s^{-1}		
	$k = 0.25$	$k = 0.5$	$k = 0.75$	$k = 0.25$	$k = 0.5$	$k = 0.75$
1	490.4	333.6	302.8	524.8	300.6	391.0
2	139.7	151.8	125.5	149.3	100.5	143.1
3	7.4	15.0	14.2	5.3	22.6	22.9
4	47.6	52.4	63.2	49.6	34.3	59.4
5	37.3	11.6	19.5	54.0	27.3	34.3
6	81.0	80.5	81.1	97.4	46.3	89.9
7	171.5	154.5	180.8	174.6	129.2	183.4
8	66.7	42.5	42.2	71.9	50.8	58.0
9	126.7	118.2	102.4	157.9	99.8	128.5
10	36.5	23.0	15.8	47.0	23.2	34.5
11	42.0	42.5	68.0	40.0	32.0	54.0

TABLE III Phase composition of the laser melted Fe–3.5 wt% C alloy

Volume fraction	Extrapolated values	$v = 8.5\ \mathrm{cm\,s^{-1}}$			Extrapolated values	$v = 17.0\ \mathrm{cm\,s^{-1}}$		
		$k = 0.25$	$k = 0.50$	$k = 0.75$		$k = 0.25$	$k = 0.50$	$k = 0.75$
ferrite	0.23	0.29	0.37	0.45	0.21	0.27	0.27	0.36
austenite	0.16	0.14	0.14	0.12	0.19	0.19	0.15	0.15
cementite	0.61	0.57	0.49	0.43	0.60	0.54	0.58	0.49

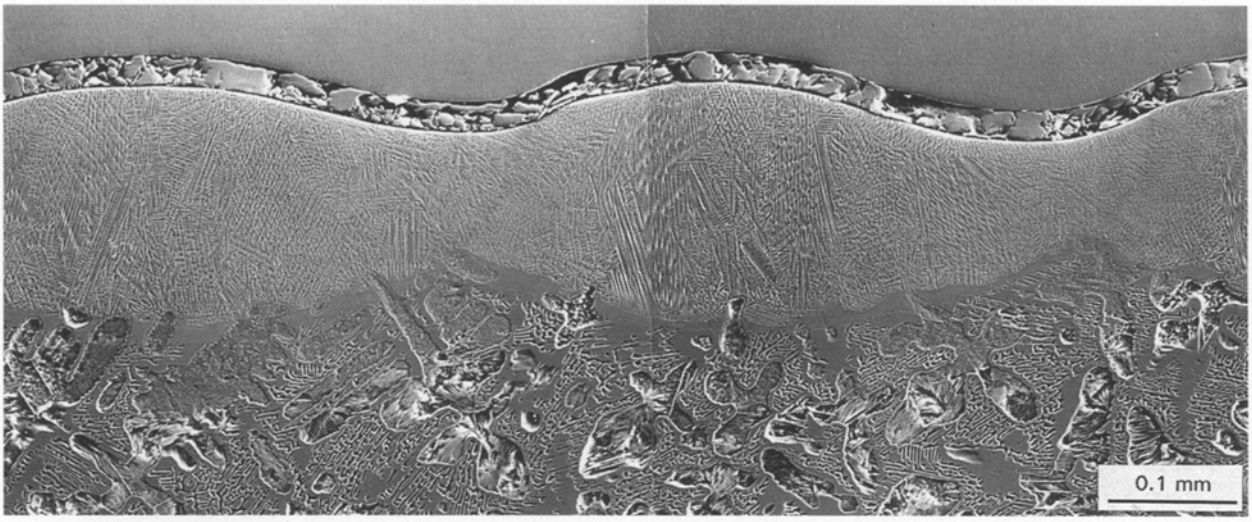

Figure 1 Cross-sectional view of overlapping laser melted tracks, $v = 8.5\ \mathrm{cm\,s^{-1}}$, $k = 0.25$.

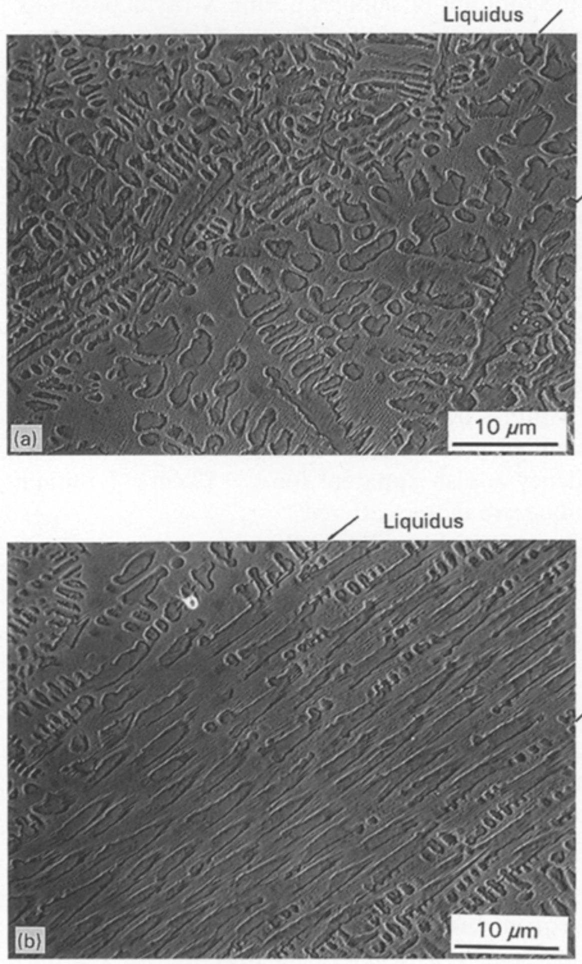

Figure 2 Structural details in the "mushy zone", $v = 8.5\ \mathrm{cm\,s^{-1}}$, $k = 0.25$. (a) Relatively coarse, equiaxed grains of primary austenite. (b) Branchless dendrites.

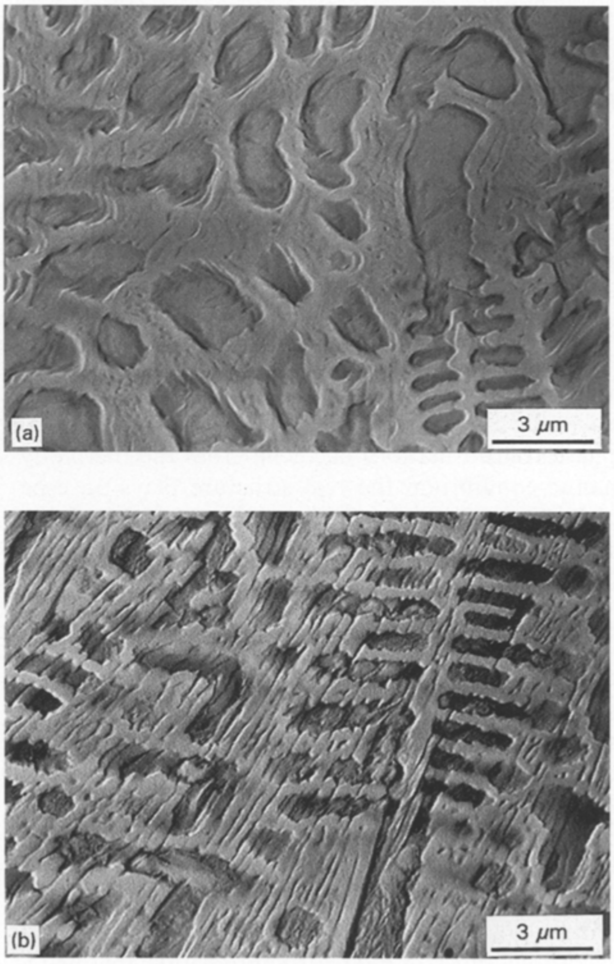

Figure 3 Different etchability of ledeburite in the "mushy zone" of one track (a) and close to the same "mushy zone" but in the preceding track (b), $v = 8.5\ \mathrm{cm\,s^{-1}}$, $k = 0.75$.

a situation analogous to that described in Part I (Section 4.5, Fig. 7) occurred. The eutectic was completely remelted while the austenite only partly melted. Since the structure in the previously melted track was very fine, the smallest austenite grains, especially the secondary dendrite arms, disappeared during the subsequent remelting. On cooling, the primary austenite obviously resolidified on the unmelted austenite remnants giving rise to the relatively coarse and branchless dendrites.

Another remarkable feature visible on the cross-sections of the superimposed passes is an increasing etchability of the ledeburite when approaching in a pass the "mushy zone" of the following pass, i.e. in the places where the heat influence of the following pass on the previously melted zone was the strongest. The situation is illustrated in Fig. 3a and b which were taken in the "mushy zone" of one track and close to the same "mushy zone" of the previous track. The difference in the carbide etchability is clearly visible.

The volume fraction of dendrites, Ω, was determined on the cross-sectional SEM micrographs using the point counting method [26], for $v = 8.5\,\mathrm{cm\,s^{-1}}$ and all three coefficients of overlapping k. The measurements were taken over several tracks in the upper part of the melted layer which was supposed to be penetrated by X-rays. The values of Ω were about 0.35, independent of k and very close to the values of Ω found for single tracks (see Fig. 6 in Part I).

5. Discussion

5.1. Effect of the real structure on the phase analysis

Results of the quantitative X-ray diffraction phase analysis depend to a great extent on the real crystal structure of the investigated samples, particularly on the size distribution of particles (regions of coherent scattering), lattice defects and on the texture in the polycrystalline aggregate. These factors can considerably influence the measured integral intensities from which concentrations of individual phases are calculated. In the laser melted surface layers where all phase transformations occur far from the thermodynamic equilibrium the real structure plays an especially important role. Typical features of the rapidly solidified structure in laser treated samples are structural gradients in a general sense and texture.

The cooling rate and the temperature gradient decrease with the depth according to the simple model of the heat propagating from a point or an area source moving with a constant speed on the surface of the sample. This is right only in the case when the streaming in the melt does not modify essentially the temperature regime. In this case, the course of the cooling rates with the depth can be just the opposite [27, 28]. In any case, conditions of solidification and phase transformations are strongly dependent on the depth under the surface.

Various types of microstructure within the melted zone, as a consequence of large temperature gradients and varying cooling rates, have been well documented, e.g. see [29, 30]. In our samples, however, no pronounced changes in the microstructure were observed by SEM when going from the outer boundary of the melted zone to its centre. On the other hand, we may expect local gradients especially in the concentration of carbon since, due to high cooling rate, the carbon atoms did not have enough time to diffuse and reach equilibrium positions of individual constituents in the resultant crystal structure. It is apparent from the detailed observations by electron microscopy described in Part I; grains of the original primary austenite (dendrites) remained partly untransformed, as a consequence of local high concentration of carbon, and partly transformed to martensite or even to pearlite. The concentration gradients result in varying interplanar spacings which in turn give rise to microstrains and to a considerable broadening of the diffraction lines. The final consequence is a significant superposition of diffraction lines. On the other hand, the small particle size (region of coherent scattering) probably did not contribute essentially to the broadening of the diffraction lines, at least not in the case of austenite.

Pronounced texture due to directional heat flow is well visible from the orientation of the dendrites within the melted zone (Fig. 1). The texture of the orthorhombic cementite was clearly apparent, e.g. from the reflection 1 3 0 of this phase. The influence of texture was to a great extent eliminated by the large number (43) of cementite reflections used for the analysis and by the rotation of samples during X-ray expositions. The superposition of the diffraction lines was respected by the choice of the method of directly including in the calculations integral intensities of the compound lines.

5.2. Effect of the laser track overlapping on the resultant phase composition

The results of X-ray diffraction for $v = 8.5\,\mathrm{cm\,s^{-1}}$ (see Table III) show clearly that the volume fraction of α-Fe in the remelted surface layers increases with increasing coefficient of track overlapping k whereas the volume fraction of carbide diminishes and the content of γ-Fe remains nearly constant. The same tendency is also apparent for $v = 17\,\mathrm{cm\,s^{-1}}$ though the data are more scattered.

The observed changes in the phase composition in relation to the coefficient k can be explained only by the effects introduced by varying geometry of overlapping. At first sight there might be two such effects:

1. different structures in the central and outer parts of the tracks; and
2. additional heat modification of the existing structure by the following adjacent — and perhaps also the second, third etc. — laser passes.

The coefficient of overlapping k was defined as the width of the streak in one track remelted by the subsequent laser pass, expressed in the width of the melted zone w as a unit. The structure for $k = 0.25$ consists of two types of alternating streaks. The broad one in the centre of the tracks is melted only once and covers 0.5 w; the outer streaks are melted twice and cover each 0.25 w. For $k = 0.75$ the final result is represented by one type of streak melted 4 times, covering 0.25 w and corresponding to the outer parts of the tracks. The X-ray measurements of the surface phase composition refer consequently, for $k = 0.25$, predominantly to the central parts of the tracks, and, for $k = 0.75$, to the outer parts. However, detailed metallographic observations on single tracks did not reveal apparent differences in the microstructure of the central and outer parts of the melted zone, so that it may be assumed with a reasonable probability that the phase composition as measured by X-ray diffraction is practically the same in the centre and near the boundaries of the tracks.

This reasoning leads to the conclusion that the changes indicated in Table III reflect the heat influence of the next pass on the preceding one in the series. This idea will be followed up in more detail. In order to quantify the thermal effect imposed by a pass on the preceding ones we shall use the heat-transfer model specified in Part I. For the constants given in Section 3, Part I, the model was shown to describe quite satisfactorily the geometry of the melted as well as austenitized zones. It may thus be assumed that the considered thermal effect will also be satisfactorily described by this model.

Fig. 4 illustates the temperature field superimposed over track 1 when the laser beam moving in the x-direction with the velocity $8.5\,\mathrm{cm\,s^{-1}}$ is creating track 2 (see the inset in Fig. 4). The temperature profiles, represented by the set of curves in Fig. 4, determine the structural changes during the thermal cycle and are thus decisive of the final microstructure and properties of the irradiated sample, as discussed, for example, in the comprehensive study by Ashby and co-workers [31, 32]. In our case, the temperature profiles were calculated for the specimen surface ($z = 0$) for various parameters $\Delta y/w$, where Δy is the distance from the melted zone boundary (i.e. from the isotherm $T_M = 1150\,^\circ\mathrm{C}$) of track 2, and w is the melted zone width. From the temperature profiles in Fig. 4 it is apparent that the structure in track 1 close to the melted zone boundary of track 2 ($\Delta y/w \simeq 0$) was exposed for a time interval $\Delta t \simeq 0.02$ s to temperatures above 500 °C. On the other hand, Fig. 4 indicates that even for the largest overlapping $k = 0.75$, the thermal effect of pass 3 on the structure in track 1 was most probably negligible: the maximum temperature in track 1 during the creation of track 3, as given by the curve for $\Delta y/w = 0.25$, did not exceed 400 °C.

Under the assumption that the changes in the phase composition with parameter k (see Table III) are caused by the subsequent very short annealing of the already melted and solidified structure by the next pass, we may try to extrapolate the data obtained from the superimposed passes to non-interfering tracks*. As depicted in Fig. 5, we consider a thin surface layer and suppose that detectable changes in the phase composition of track 1 could occur in the region where the maximum temperature during the subsequent pass 2 was higher than a certain temperature T_{an}. The changes will be greatest close to the T_M boundary and will diminish when approaching T_{an}, the average change in the volume fraction of a phase in this region being $\overline{\Delta\Phi}$. For the total volume fraction Φ of the phase as measured by X-ray diffraction it follows:

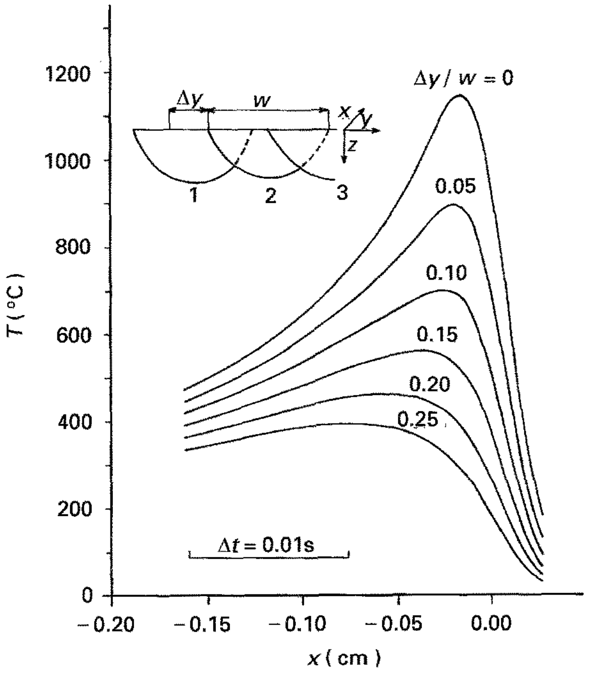

Figure 4 Temperature field superimposed by pass 2 over track 1 (see the inset) calculated for $v = 8.5\,\mathrm{cm\,s^{-1}}$. Position $x = 0$ corresponds to the centre of a Gaussian beam moving in the x-direction.

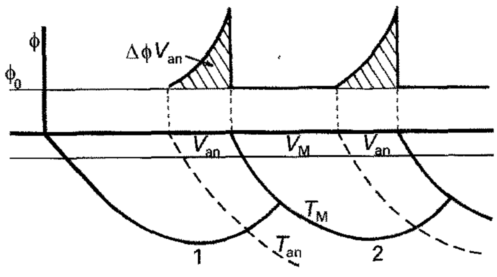

Figure 5 Outline of changes in the phase composition due to tempering of one track by the subsequent laser pass. For explanation see the text.

$$\Phi = \frac{\Phi_0 V_M + (\Phi_0 + \overline{\Delta\Phi}) V_{an}}{V_M + V_{an}} =$$

$$= \Phi_0 + \overline{\Delta\Phi}\,\frac{V_{an}}{V_M + V_{an}} = \Phi_0 + \overline{\Delta\Phi}\,p \quad (7)$$

where V_{an} and V_M are the volumes of the thermally influenced and uninfluenced portions of the layer, respectively, and Φ_0 is the volume fraction of the considered phase in the thermally uninfluenced parts. The parameter $p = V_{an}/(V_M + V_{an})$ represents the

---

*It is evident that experiments even with $k = 0$ could not create "non-interfering" tracks. In that case, the following pass would not remelt the preceding one, however, a heat-affection would not be avoided at all.

volume fraction of the thermally influenced parts in the layer and is related to the coefficient of overlapping k by the expression $p = w_{an}/w\ (1 - k)$, (w_{an} = the width of the thermally influenced parts).

In Fig. 6 the measured volume fractions Φ_α, Φ_γ and Φ_C of α-Fe, γ-Fe and carbide, respectively (see Table III) are plotted versus parameter p estimated for $T_{an} = 500\,^\circ C$. While the volume fraction of γ-Fe seems to be nearly constant, the contents of α-Fe and cementite change considerably with the parameter p. The changes in Φ_α and Φ_C are more pronounced for $v = 8.5\ \mathrm{cm\,s^{-1}}$ than for $v = 17\ \mathrm{cm\,s^{-1}}$ which would correspond to a longer annealing time at the lower scanning speed. A linear extrapolation to $p \to 0$ gives similar values for both scanning speeds and points to $\Phi_{\alpha 0} \simeq 0.22$; $\Phi_{\gamma 0} \simeq 0.18$ and $\Phi_{C0} \simeq 0.60$ for the thermally uninfluenced, i.e. single tracks. These values were used for the discussion in Part I.

The simple model suggested for the extrapolation $p \to 0$ for any scanning velocity assumes exactly the same value $\overline{\Delta\Phi}$ for any coefficient of overlapping and the real temperature of annealing does not enter into the process of extrapolation. Thus, the limiting temperature $T_{an} = 500\,^\circ C$ used in the extrapolation procedure has been chosen rather arbitrarily. However, the suggested linear regression may prove its practical value in individual measurements as for example here and is suitable as the first test before more complicated models are applied. It is interesting to state that, for example, a regression exponential term of the form ab^x yields practically the same results as the linear procedure.

The linear regression analysis, performed for all three structure components and both velocities on the basis of experimental data presented in Table III, yielded the extrapolated values also included in Table III. Comparison of the extrapolated high volume fractions of cementite 0.61 and 0.60, respectively, for both velocities with the equilibrium value of 0.53 in the system Fe–3.5 wt% C indicates clearly statistically significant differences. The indicated values are thus taken as a proved reality.

5.3. Structure and stability of cementite

Of the metastable iron–carbon compounds the most important is cementite, a phase that plays an essential role in the hardening of many commercial steels [33]. The exact data necessary for calculations of intensity factors in Section 3 were taken from [15]. Structure data on cementite are not strictly unified because of the difficulties arising from the properties of this compound [33, 34]. An account of such difficulties may be documented as follows:

1. The problem of stability is very general. Additions of Mn and Cr stabilize the cementite structure to the point that large (≃ 100 μm) single crystals can be grown. The most precise determination to date of the cementite structure was just based on single crystal X-ray diffraction data from a stable $(Fe_{0.9}Mn_{0.1})_3C$ phase [35]. Unfortunately, structure data referring to these stabilized carbides cannot sometimes be avoided for the binary system due to a lack of other information.

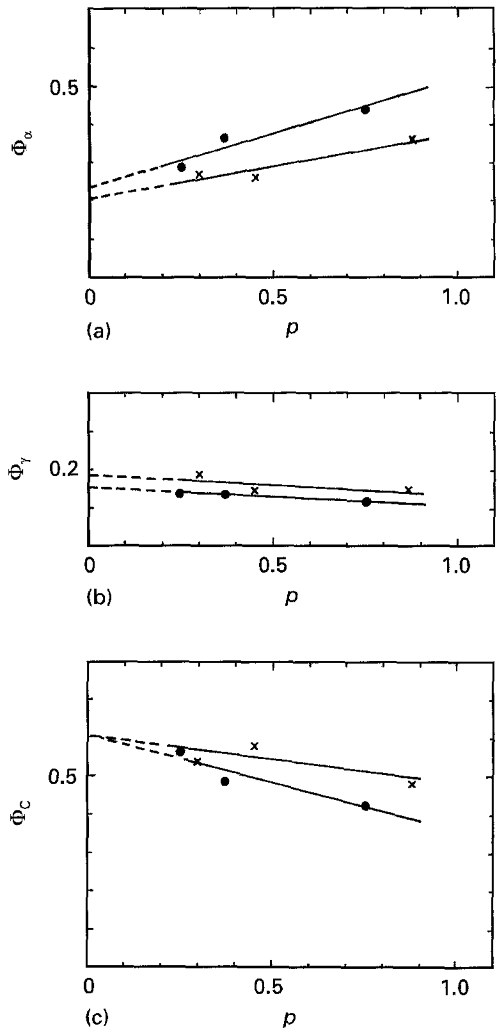

Figure 6 Volume fraction of α-Fe (a), γ-Fe (b) and carbide (c) as functions of parameter p for $T_{an} = 500\,^\circ C$. The extrapolated values ($p = 0$) correspond to non-interfering laser passes. ●, $v = 8.5\ \mathrm{cm\,s^{-1}}$ and ×, $v = 17\ \mathrm{cm\,s^{-1}}$.

2. On cooling the Fe–C system, the metastable cementite forms at ≃ 1147 °C and in the reverse direction, on heating, it starts to decompose at 500 °C [36]. This irreversible behaviour is especially important in pulse annealing of the melted zone by the next laser pass. It is reasonable to assume that the temperature of decomposition depends on stoichiometry and represents no firm constant. On the contrary, annealing for several hours near the point of decomposition stabilizes cementite. This effect is accompanied by a decrease of the Curie temperature [37].

3. The major problem in all considerations is the stoichiometric composition depending strongly on conditions of formation of cementite and determining its structural characteristics and thermodynamic properties.

Petch [38] measured lattice parameters of cementite as a function of the quenching temperature and found a decrease ≃ 0.18% of the elementary cell volume for the quenching temperature 900 °C as compared to the slowly cooled material. This decrease suggested lower content of interstitial carbon in the framework of metal atoms. Fruchart *et al.* [39] report on analogical studies on the isomorph structure Pd_3P with a much higher variation, $\simeq 4\%$, of the elementary cell volume attributed to the vacancy structure of phosphorus atoms in Pd_3P.

There are numerous papers on carbides with the ratio Fe:C < 3 in the binary system Fe–C (see review [33]), but the present authors have not found any paper on the exact relation between lattice parameters and carbon content in cementite for Fe:C > 3 (presence of carbon vacancies). The generally accepted pleated sheet concept of the structure of cementite, first introduced in [35], restores carbon to the role of an interstitial atom in a recognizable metal–atom framework [33] evidently giving space to a higher fraction of carbon vacancies similarly as in ε-carbide. Papers [23, 24, 40–42] on splat quenching and laser treatment generally indicate wide limits in stoichiometry of ε-phase and ε-carbide, if they mention them, but direct data for cementite are systematically missing.

5.4. Analysis of the measured values

In the light of past considerations the results in Table III may be summarized as follows.

The predominant component for both velocities is cementite with volume fractions $\Phi_C \simeq 0.60$. The reasoning explained in Part I, Section 5, led to an estimate of the carbon content available for carbide formation of $\simeq 3.0$ wt% and consequently to the theoretical equilibrium content of cementite $\simeq 0.45$ as the lower limit. Taking volume fraction $\Phi_C = 0.60$ as measured in the laser treated material, one obtains for the effective stoichiometry of carbon in cementite the value $s = 0.75$ compared to $s = 1$ in the perfect lattice. This corresponds to the composition $\simeq Fe_4C$. Volume fractions Φ_C and Φ_α decrease and increase, respectively, with higher overlapping for both velocities. It can be stated that the increasing coefficient k leads to a decomposition of the non-stoichiometric cementite by annealing pulses of different temperature versus time profiles (Fig. 4). Duration of pulses is $\simeq 10^{-2}$ s according to the distance $\Delta y/w$ from the melted zone.

A strongly simplified carbon balance may now be tried on the basis of the general requirement of conservation of the total quantity of carbon. Pulse annealing reduces the volume fraction of cementite and the "free" carbon which results as a product of the decomposition may, in principle, either form graphite (as recently described in [42]) or enter different compounds of the system. Contrary to [42] no graphite was observed on the metallographic micrographs. The solubility of carbon in ferrite is negligible. On the other hand, dissolution of cementite in austenite above the austenitizing temperature and subsequent trapping of carbon in austenite should be taken into account. In that case the volume fraction of γ-Fe would be expected to increase with increasing overlapping. However, the volume fraction of austenite Φ_γ is practically independent of the coefficient of overlapping k and approximately equal for both scanning velocities. It may thus be assumed that all "free" carbon, or at least the main proportion of it, will enter the lattice of the remaining non-stoichiometric cementite and that the two processes will occur simultaneously: decomposition of part of the cementite; and saturation and recovery of the rest.

The conservation of the total quantity of carbon after the two processes may be expressed by the relation

$$\Phi_1 s_1 = \Phi_2 s_2 \qquad (8)$$

The subscripts 1 and 2 refer to the state before and after the mentioned processes, respectively, Φ denotes the volume fraction of the considered phase (cementite) and s the stoichiometry of carbon. Equation 8 may include on both sides several terms for several structural components. Referring the subscript 1 to the extrapolated value $\Phi_1 = 0.61$ and to the estimated stoichiometry $s = 0.75$ (see above), one finds from Equation 8 for $v = 8.5\ \mathrm{cm\,s^{-1}}$ and coefficients of overlapping $k = 0.25, 0.5$ and 0.75, values of $s_2 = 0.80, 0.93$ and 1.06, respectively. The trend of the values s_2 seems reasonable and corresponds to the increasing decomposed fraction of cementite. The linear relationship between s_2 and k is surprising and unexpected and will be the subject of further consideration.

The idea of partial decomposition and partial recovery of cementite during annealing pulses rests upon two statements in [36] and [37]. Simultaneous presence of these two processes assumes only short-path diffusion of carbon. Further investigations along these lines are necessary to support or reject the suggested idea and to bring a deeper insight into the possible simultaneous processes.

6. Conclusions

X-ray diffraction was applied to a quantitative phase analysis of the identified components α-Fe, γ-Fe and cementite in laser melted surface layers of Fe–3.5 wt% C.

1. The volume fraction of austenite did not change significantly with the coefficient of overlapping and scanning velocity.
2. Cementite decomposed with increasing overlapping, i.e. with increasing effect of annealing pulses from the adjacent laser passes.
3. Carbon as the product of decomposition is assumed to contribute to the stoichiometry of the remaining partially recovered cementite.
4. The higher scanning velocity reduced the rate of decomposition of the cementite because of the shorter annealing pulses.

Acknowledgements

The authors are grateful to Dr J. Fiala and Dr J. Lašek for valuable comments on the manuscript. This research was funded by the Grant Agency of the Academy of Sciences of the Czech Republic under grant No. 11047 and this support is gratefully acknowledged.

References

1. M. GREMAUD, M. CARRARD and W. KURZ, *Acta Metall. Mater.* **39** (1991) 1431.
2. M. RIABKINA-FISHMAN, J. ZAHAVI and L. S. ZEVIN, *J. Mater. Res.* **3** (1988) 1108.
3. M. RIABKINA-FISHMAN, L. S. ZEVIN and J. ZAHAVI, *J. Mater. Sci. Lett.* **7** (1988) 741.
4. N. GANEV, I. KRAUS and J. TRPČEVSKÁ, *Phys. Status Solidi (a)* **115** (1989) K13.
5. I. KRAUS, N. GANEV and J. TRPČEVSKÁ, *Kovové Materiály* **28** (1990) 513.
6. M. CHACHALÁK and J. TRPČEVSKÁ, *ibid.* **29** (1991) 429.
7. R. KRÁLOVÁ, *J. Mater. Sci. Lett.* **12** (1993) 1951.
8. R. KRÁLOVÁ, *Mater. Sci. Eng.* **A174** (1994) L51.
9. M. CARBUCICCHIO, G. MEAZZA, G. PALOMBARINI and G. SAMBOGNA, *J. Mater. Sci.* **18** (1983) 1543.
10. A. WALKER, H. M. FLOWER and D. R. F. WEST, *ibid.* **20** (1985) 989.
11. F. FOUQUET and E. SZMATULA, *Mater. Sci. Eng.* **98** (1988) 305.
12. B. D. CULLITY, in "Elements of X-Ray Diffraction" (Addision-Wesley, Reading, Massachusetts 1956) p. 392.
13. G. FANINGER and U. HARTMAN, *Härterei-Techn. Mitt.* **27** (1972) 233.
14. J. FIALA, *Kovové Materiály* **6** (1968) 579.
15. R. W. G. WYCKOFF, in "Crystal Structures", Vol. **2**, 2nd Edn (J. Wiley, New York, 1964) pp. 112–115.
16. A. TAYLOR, in "X-Ray Metallography" (J. Wiley, New York 1960) p. 249.
17. H. FABER and U. HARTMAN, *Härterei-Techn. Mitt.*, **38** (1975) 238.
18. J. FIALA, *Silikáty* **29** (1985) 273.
19. U. HARTMAN, *Härterei-Techn. Mitt.* **27** (1972) 251.
20. L. E. EISELSTEIN, O. A. RUANO and O. D. SHERBY, *J. Mater. Sci.* **18** (1983) 483.
21. S. NAGAKURA, *J. Phys. Soc. Japan* **14** (1959) 186.
22. R. C. RUHL and M. COHEN, *Acta metall.* **15** (1967) 159.
23. *Idem*, Trans. Met. Soc. AIME **245** (1969) 241.
24. J. M. DUBOIS and G. LE CAER, *Acta metall.* **25** (1977) 609.
25. I. R. SARE, *J. Mater. Sci.* **16** (1981) 3470.
26. E. R. WEIBEL, in "Stereological Methods", Vol. 1 (Academic Press, London, 1979).
27. N. ZÁRUBOVÁ, V. KRAUS and J. ČERMÁK, *J. Mater. Sci.* **27** (1992) 3487.
28. J. ČERMÁK, M. ČERŇANSKÝ, P. WOLF and N. ZÁRUBOVÁ, in 13th General Conference of the Condensed Matter Division of the European Physical Society, Regensburg, Germany, 29 March–2 April 1993, *Europhysics Conference Abstracts* **17A** (1993) 1264.
29. L. E. GREENWALD, E. M. BREINAN and B. H. KEAR, in "Laser-Solid Interactions and Laser Processing", edited by S. D. Ferris, H. J. Leamy and J. M. Poate (American Institute of Physics, New York, 1979) p. 189.
30. S. C. GILL, M. ZIMMERMANN and W. KURZ, *Acta Metall. Mater.* **40** (1992) 2895.
31. M. F. ASHBY and K. E. EASTERLING, *Acta Metall.* **32** (1984) 1935.
32. J. C. ION, K. E. EASTERLING and M. F. ASHBY, *ibid.* **32** (1984) 1949.
33. H. L. YAKEL, *Int. Met. Rev.* **3** (1985) 17.
34. G. LE CAER and S. BAUER-GROSSE, *Hyperfine Interactions* **47** (1989) 55.
35. E. J. FASISKA and G. A. JEFFREY, *Acta Crystallogr.* **19** (1965) 463.
36. H. SCHUMANN, in "Metallographie", 11. Auflage (VEB Deutscher Verlag für Grundstoffindustrie, Leipzig, 1983) p.314.
37. W. STUCKENS and A. MICHEL, *Comptes Rendus* **253** (1961) 2358.
38. N. J. PETCH *J. Iron Steel Inst.* **149** (1944) 143.
39. E. FRUCHART, R. FRUCHART and A. MICHEL, *Comptes Rendus* **252** (1961) 3263.
40. P. G. BOSWELL and G. A CHADWICK, *J. Mater. Sci.* **11** (1976) 2287.
41. A. AMULYAVICHYUS, M. BALCHYUNENE, S. GRIGALYUNAS and B. PETRETIS, *Fyz. Met. Metallovedenije* **76** (1963) 94.
42. H. M. WANG and H. W. BERGMANN, *Scripta Met. Mater.* **31** (1994) 433.

Received 6 September 1994
and accepted 17 July 1995